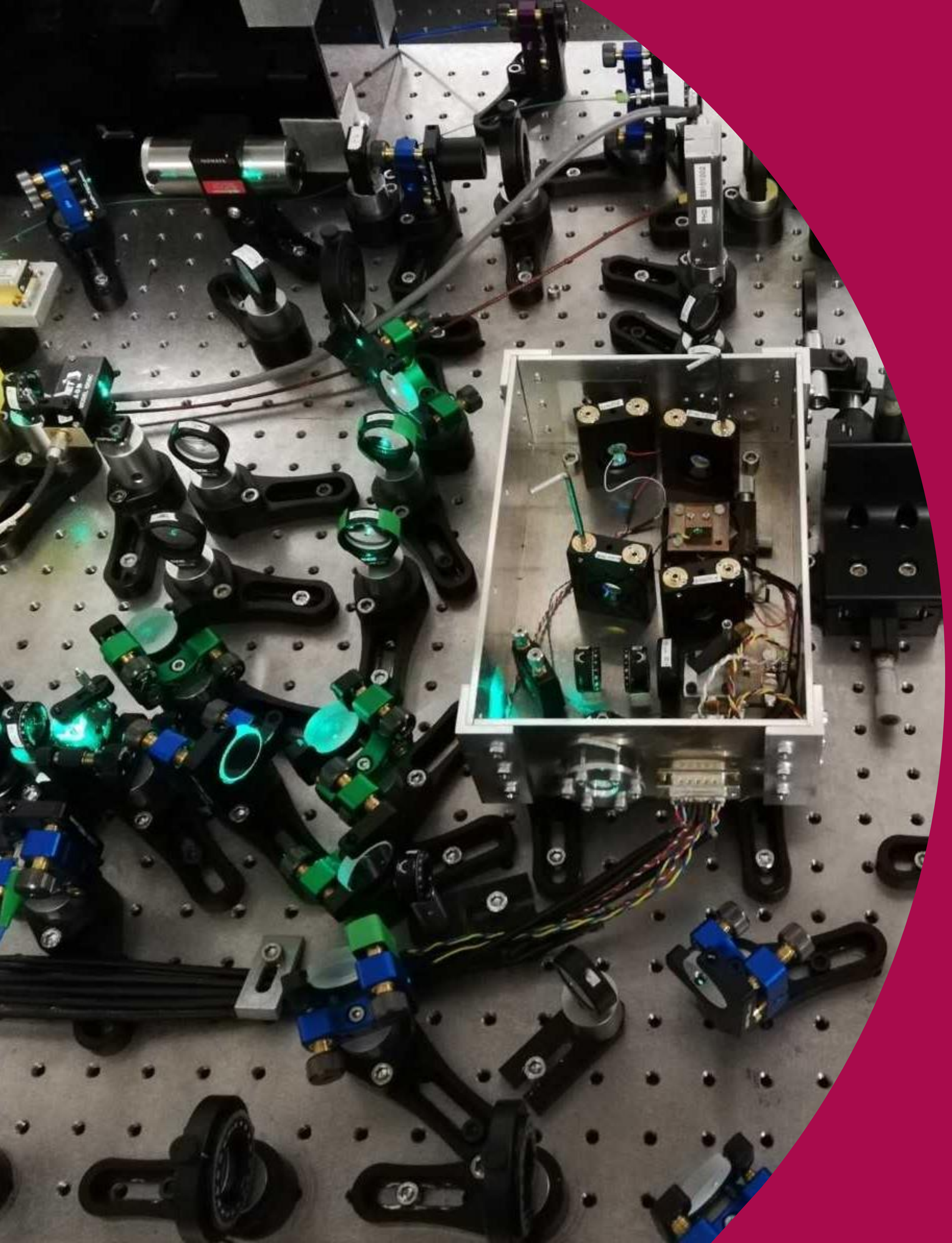

Comb-assisted Lamb-dip spectroscopy of the mercury intercombination line at 253.7 nm for metrological applications

Stefania Gravina, Naveed A. Chishti, Simona Di Bernardo and Livio Gianfrani

Dipartimento di Matematica e Fisica, Università degli Studi della Campania "Luigi Vanvitelli", Caserta, Italy

Interests

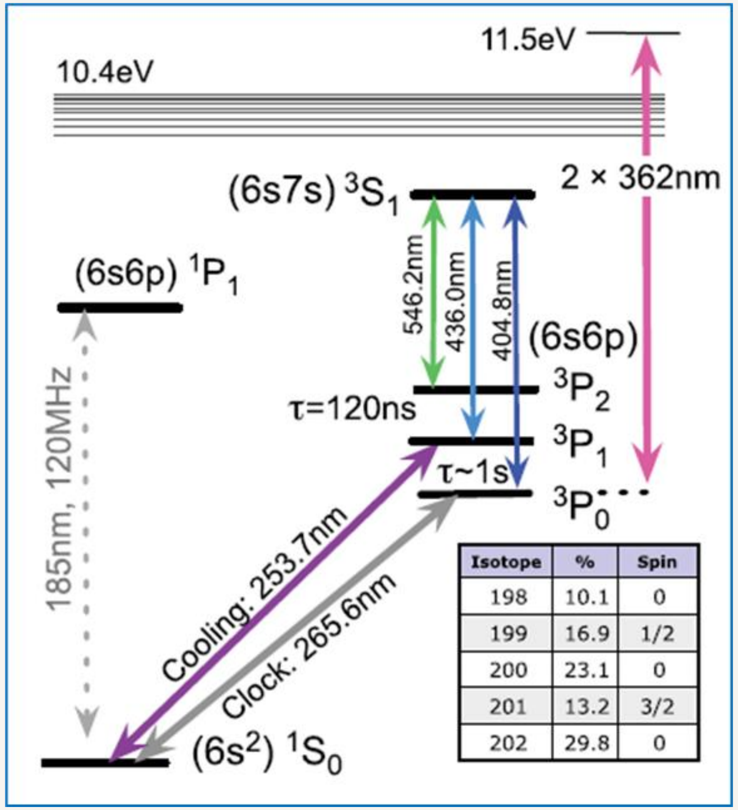

Isotope	%	Spin
198	10.1	0
199	16.9	1/2
200	23.1	0
201	13.2	3/2
202	29.8	0

Metrology

Laser cooling and trapping of mercury vapours for an optical lattice clock;

Doppler Broadening Thermometry for the implementation of the new kelvin.

«New physics» experiments

Search for a permanent electric dipole moment of the ^{199}Hg atom;

Possible long-term variations of the fine structure constant.

Environmental monitoring for health protection

Spectroscopic determination of absolute concentrations of gaseous elemental mercury in air.

Astrophysics

Overabundances and isotope anomalies of mercury in HgMn stars.

Motivations

Temperature metrology

The Doppler Broadening Thermometry (DBT) consists in measuring very precisely the Doppler width of an absorption profile corresponding to an isolated atomic or molecular spectral line in a gas at the thermodynamic equilibrium.

Gas particles with random motion

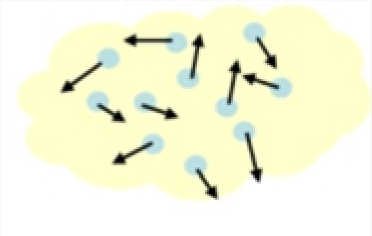

$$\Delta\nu_D = \sqrt{\ln 2}\,\nu_0\sqrt{2\frac{k_B T}{Mc^2}}$$

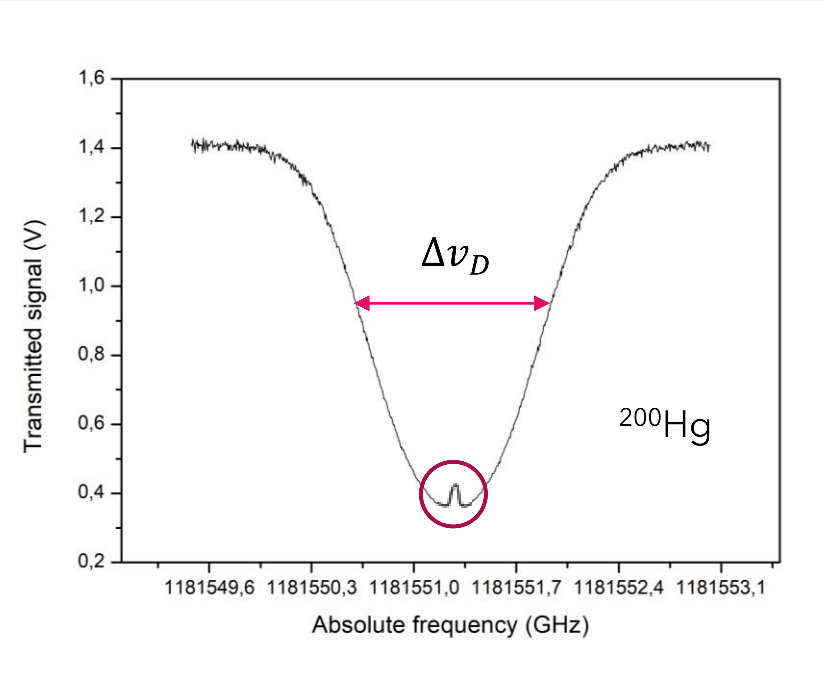

Mercury atoms for DBT

- ✓ seven stable isotopes, five of which having zero nuclear spin;
- ✓ vapor pressure at TPW temperature = 0.026 Pa (orders of magnitude larger than that of Rb or Cs);
- ✓ large Doppler width;
- ✓ collisional perturbations to the line profile can be completely neglected.

Objectives

- ➢ **High precision measurements of the center frequency of the mercury intercombination line;**
- ➢ **Improvements of the current knowledge of the ^{200}Hg-^{202}Hg isotope shift of this spectral line.**

S. Gravina, et al. Phys. Rev. Res. **4**, 033240 (2022).
S. Gravina, et al. *Journal of Physics: Conference Series*, **2439** (1), 012015 (2023).

Experimental apparatus

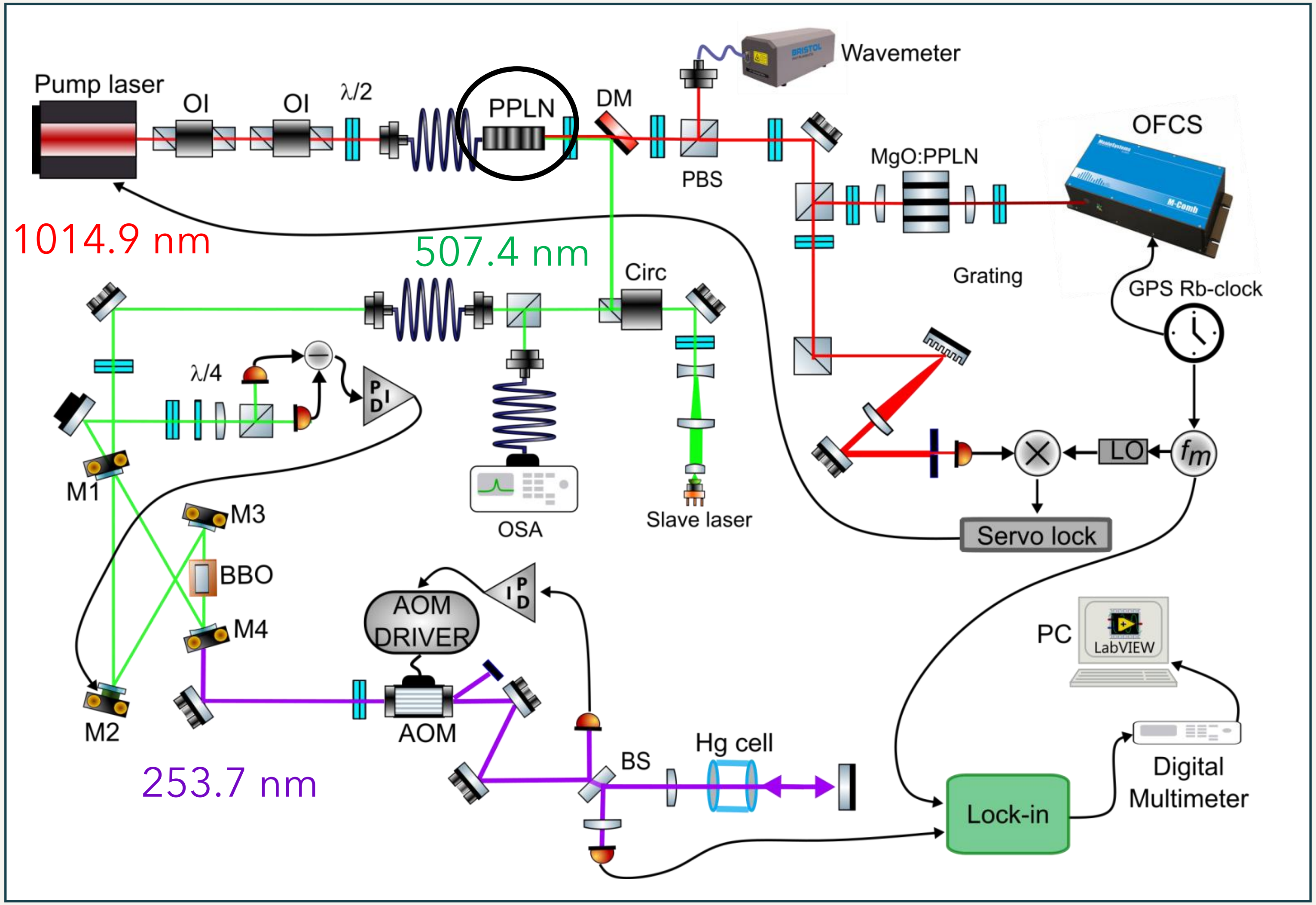

First stage of Second harmonic Generation:

1014.9 nm → 507.4 nm

using a fiber-coupled periodically poled lithium niobate (PPLN) crystal waveguide

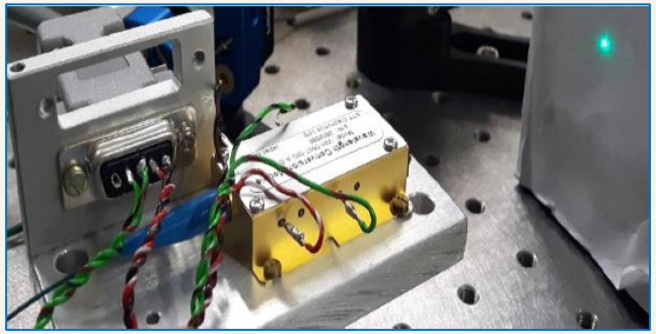

Clivati, C., Gravina, S., Castrillo, A., Costanzo, G. A., Levi, F., & Gianfrani, L. (2020). Optics Letters, **45**(13), 3693-3696.

Experimental apparatus

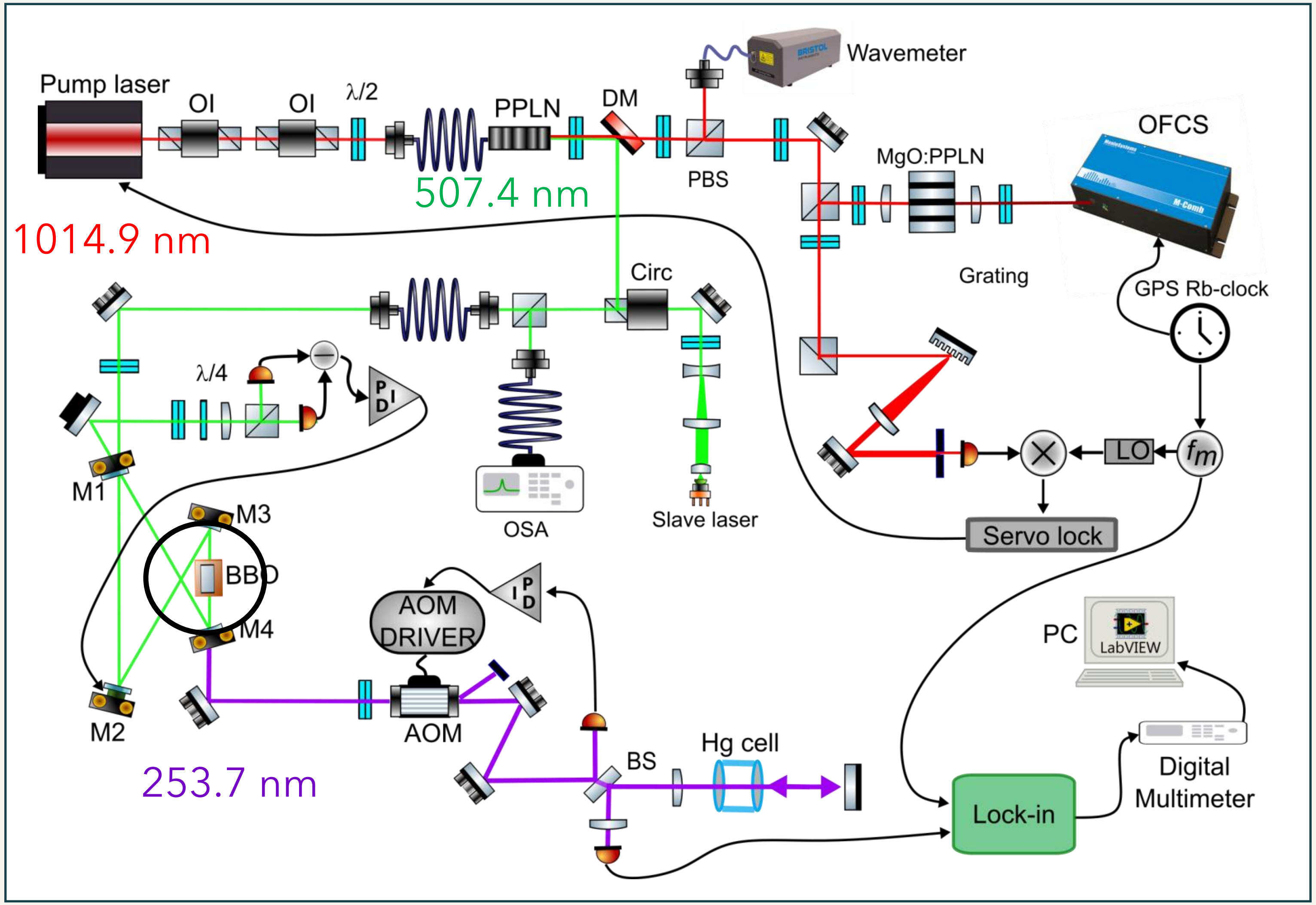

Second stage of Second harmonic Generation:

507.4 nm → 253.7 nm

through a 12 mm long beta-barium borate (BBO) crystal placed inside a bow-tie resonant cavity, locked to the incoming beam through the Hänsch-Couillaud technique.

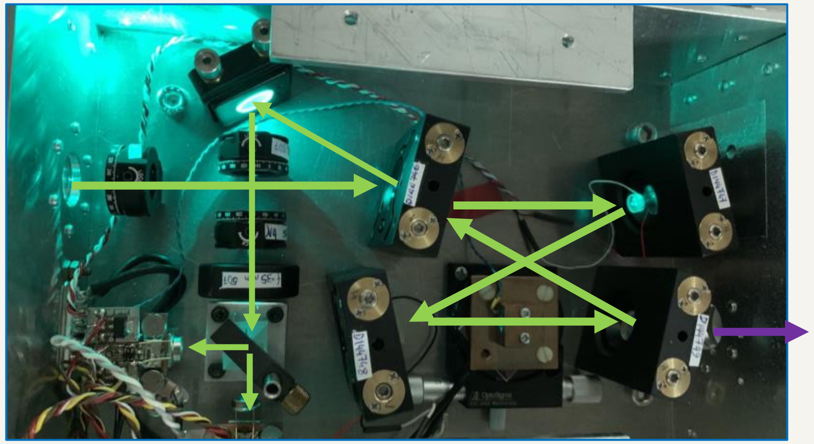

Clivati, C., Gravina, S., Castrillo, A., Costanzo, G. A., Levi, F., & Gianfrani, L. (2020). Optics Letters, **45**(13), 3693-3696.

Experimental apparatus

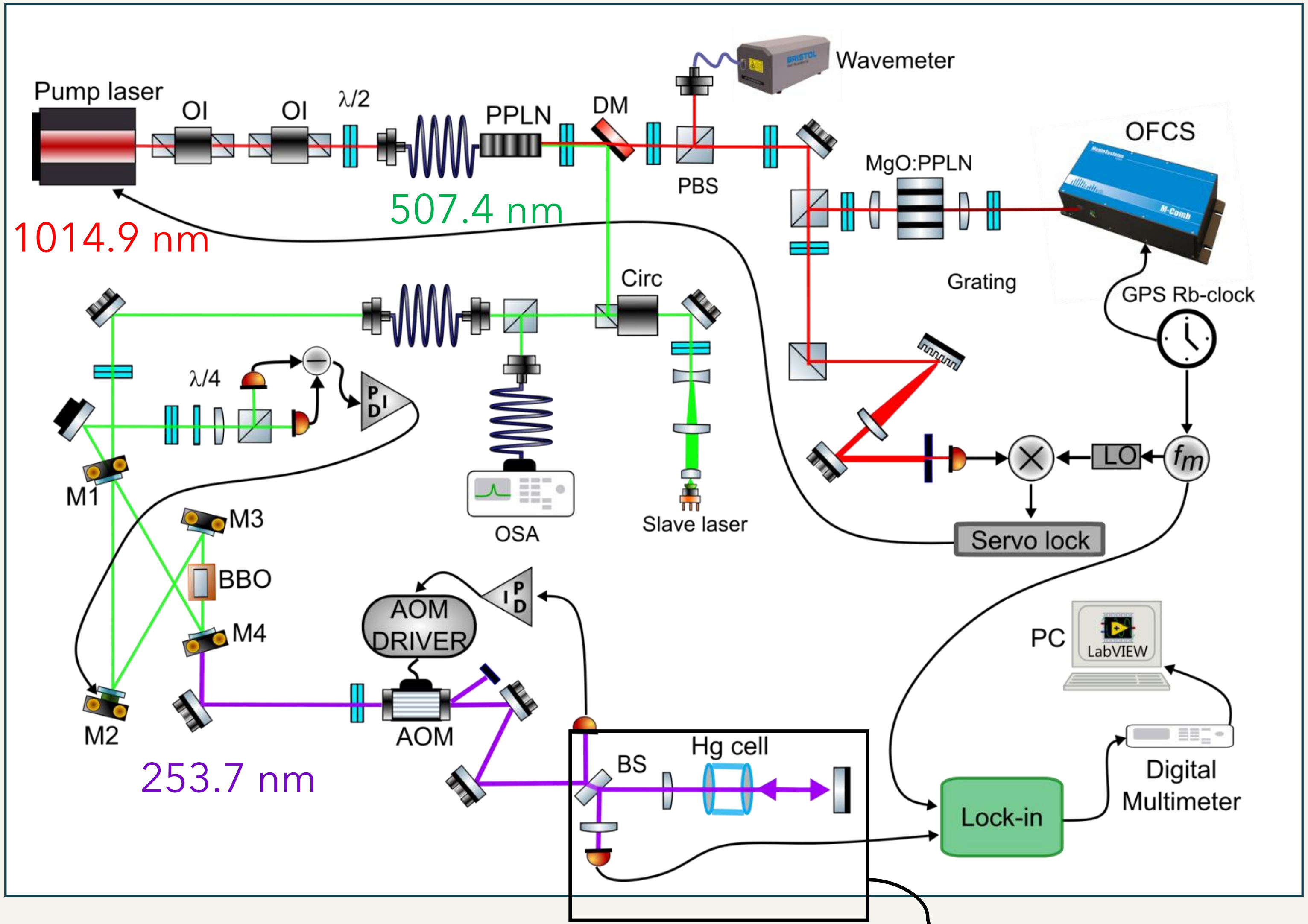

Window material Spectrosil®
Quartz short pathlength cell
(1.00±0.01) mm

$\Delta P_t / P_{in}$ = 9%
at 273.15 K

The cell is baked at 425°C for a minimum of 24 hours in an ultra-high vacuum environment prior to any introduction of mercury in the reservoir.

Pump and probe scheme

Comb referencing of the UV source

Second Harmonic Generation of the Optical frequency comb synthesizer (from Menlo Systems) wavelength portion at 2 μm using a 3 mm long Magnesium doped Lithium Niobate (MgO: PPLN) crystal.

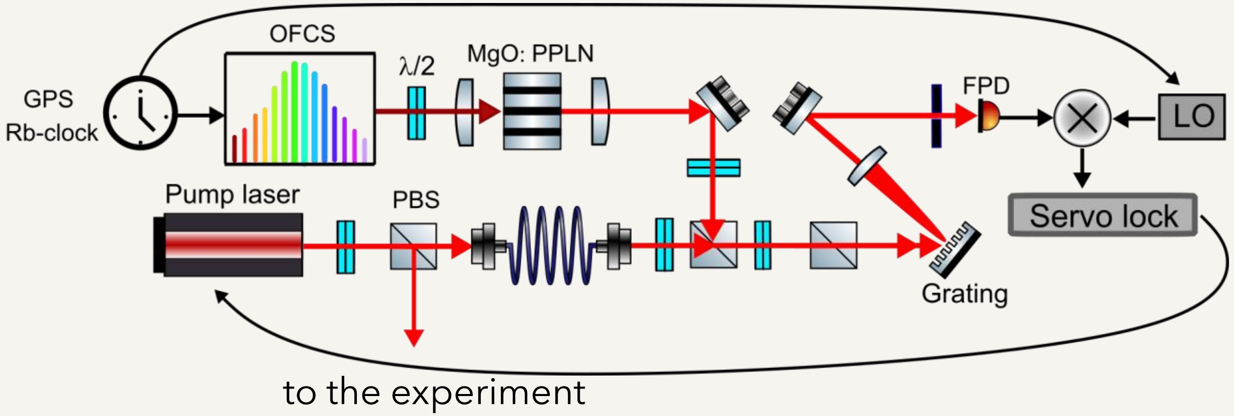

Mini-comb centred at 1020 nm
with a peak power of about 1.5 μW at the resolution bandwidth of 1 nm

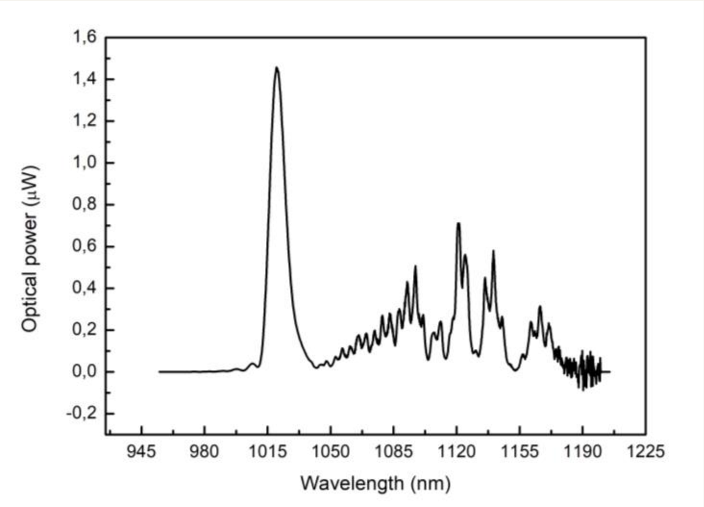

Comb-locked configuration

$$\nu_{UV} = 4 \times (\pm f_{beat} + N f_{rep} \pm 2 f_{ceo})$$

f_{rep} the repetition rate (250 MHz)
f_{ceo} the carrier-envelope offset frequency (20 MHz)

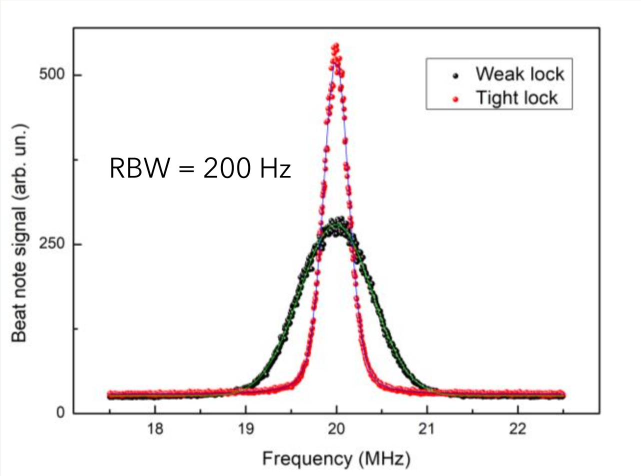

Doppler-free saturation spectroscopy

Wavelength modulation technique

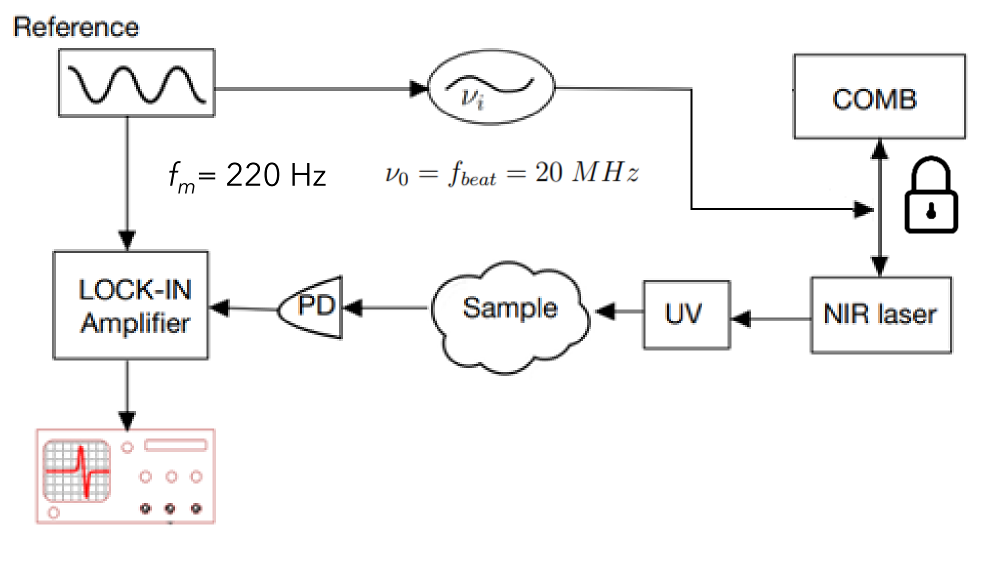

Frequency scan

- Number of points= 500;
- Acquisition time = 77 s;
- Frequency step= 48 kHz.

Δf_{rep}=5 Hz → $\Delta\nu_{NIR}$ = 6 MHz → $\Delta\nu_{UV}$=24 MHz

Example of the dispersive ^{200}Hg sub-Doppler spectrum

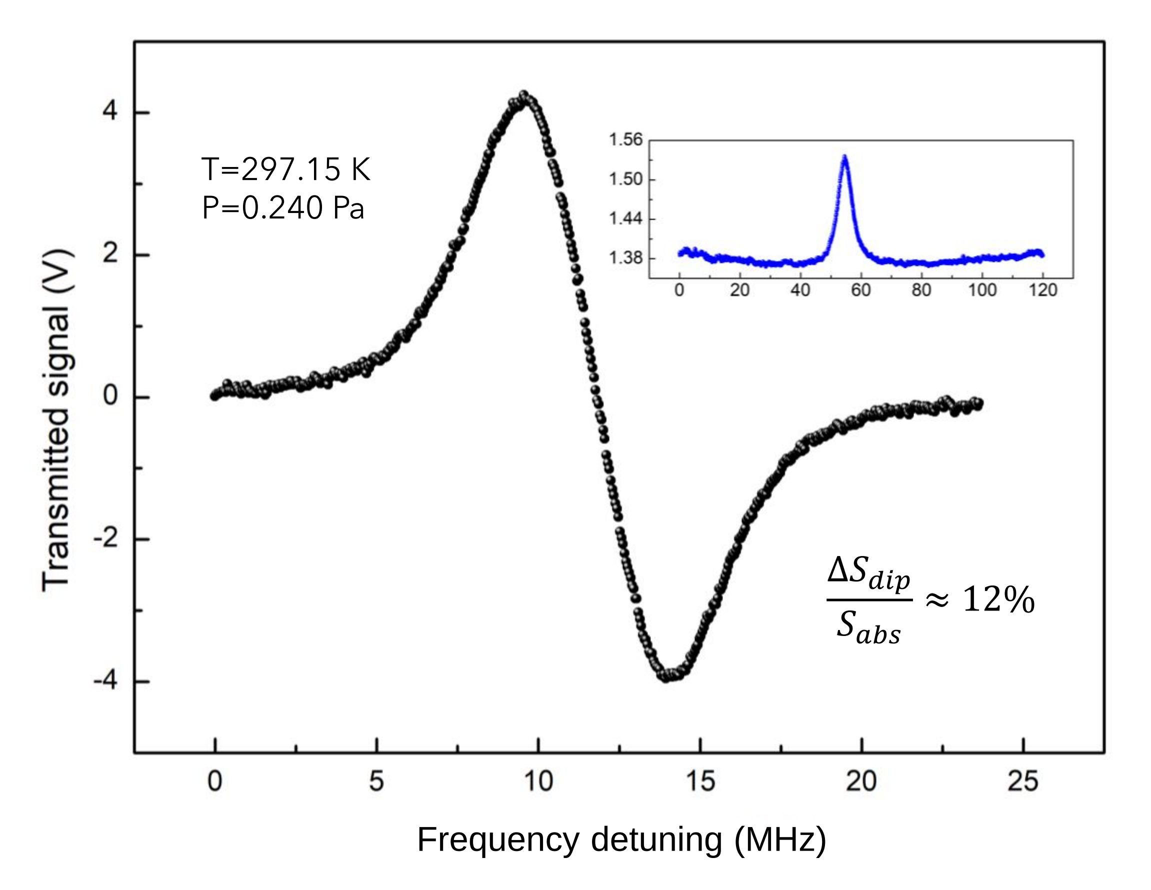

Modulation index~1

$I \approx 250\ W/m^2$

The Lamb-dip is no longer limited by the Doppler effect.

Spectral analysis

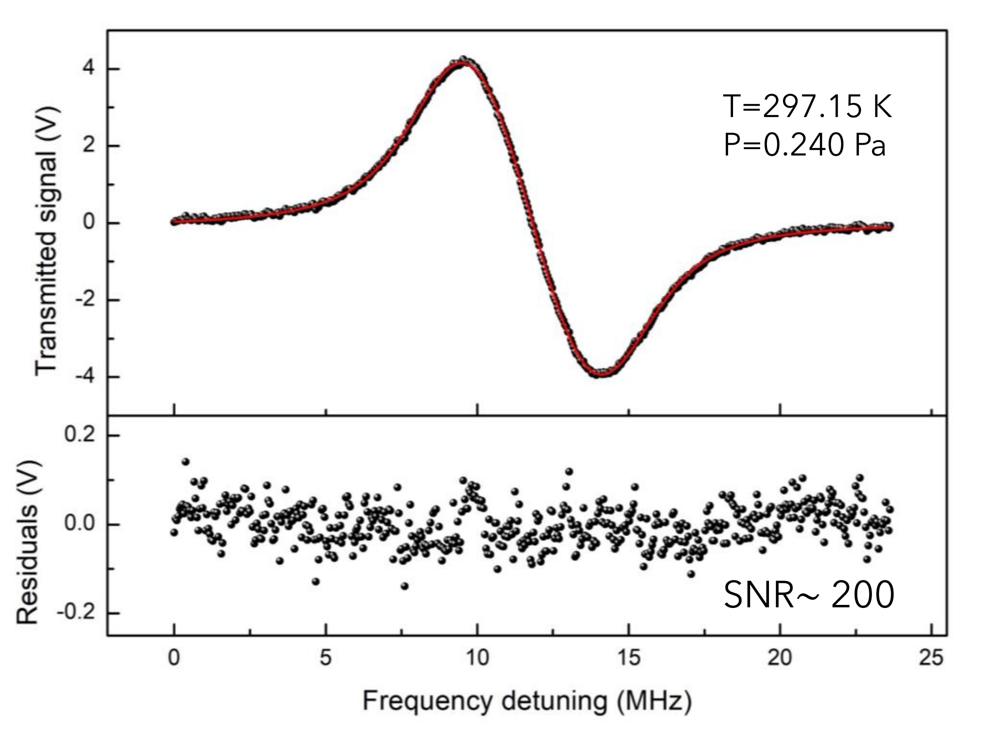

Residuals obtained by using a normal first derivative of the Voigt function

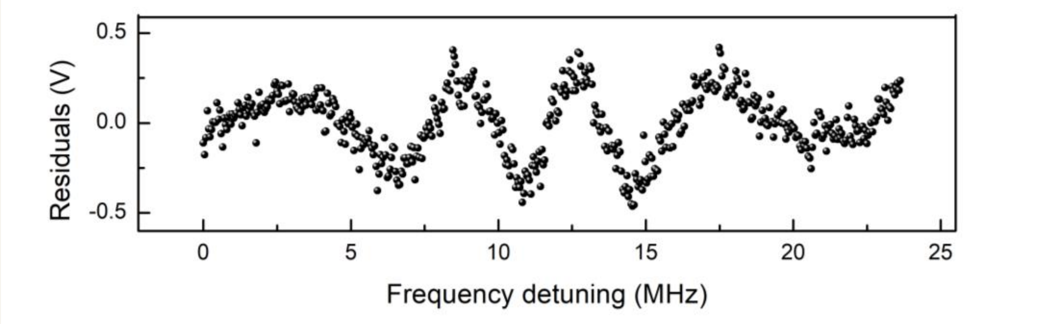

Line-shape model: Wavelength-modulated Lamb-dip Voigt function

$$S_{V,n}^{in} = -\beta\eta I_0 S n_a L \times \chi_{V,n}^{even}(\bar{\nu}_d, \bar{\nu}_a)$$

even component of the n^th Fourier coefficient of the wavelength modulated Voigt

- β gain of the lock-in amplifier;
- η detector sensitivity;
- I_0 incident light intensity;
- S integrated line strength;
- n_a density of absorber;
- L interaction length;
- $\bar{\nu}_d$ normalized detuning frequency;
- $\bar{\nu}_a$ modulation amplitude;
- y ratio of the Lorentzian and Gaussian widths multiplied by $\sqrt{\ln 2}$.

Westberg-Wang-Axner methodology

$$\chi_{V,n}^{even}(\bar{\nu}_d, \bar{\nu}_a) = \frac{y}{\pi^{3/2}\delta\nu_L} \times \int_{-\infty}^{+\infty} \frac{2}{\tau} \int_0^{\tau} \frac{\cos(2\pi n f_m t)dt}{1 + [(\bar{\nu}_d + s') + \bar{\nu}_a \cos(2\pi n f_m t)]^2} \times e^{-y^2 s'^2} ds'$$

$$\chi_{V,n}^{even}(\bar{\nu}_d, \bar{\nu}_a) = \frac{y}{\pi^{1/2}} \times \int_{-\infty}^{+\infty} \chi_{L,n}^{even}(\bar{\nu}_d + s', \bar{\nu}_a) e^{-y^2 s'^2} ds'$$

$$S_{V,1}^{in}(\nu_{UV} - \nu_0) = P_0 + P_1 \times G_D(\nu_{UV} - \nu_0) + \beta' \chi_{V,1}^{even}(\bar{\nu}_d, \bar{\nu}_a)$$

First derivative of the Gaussian function with the Doppler width fixed at the measured value of the gas temperature.

FWHM sub-Doppler line ~ 4.4 MHz

J. Westberg, J. Wang, and O. Axner, J Quant Spectrosc Radiat Transf **113,** 2049-2057 (2012).

Absolute frequency measurements

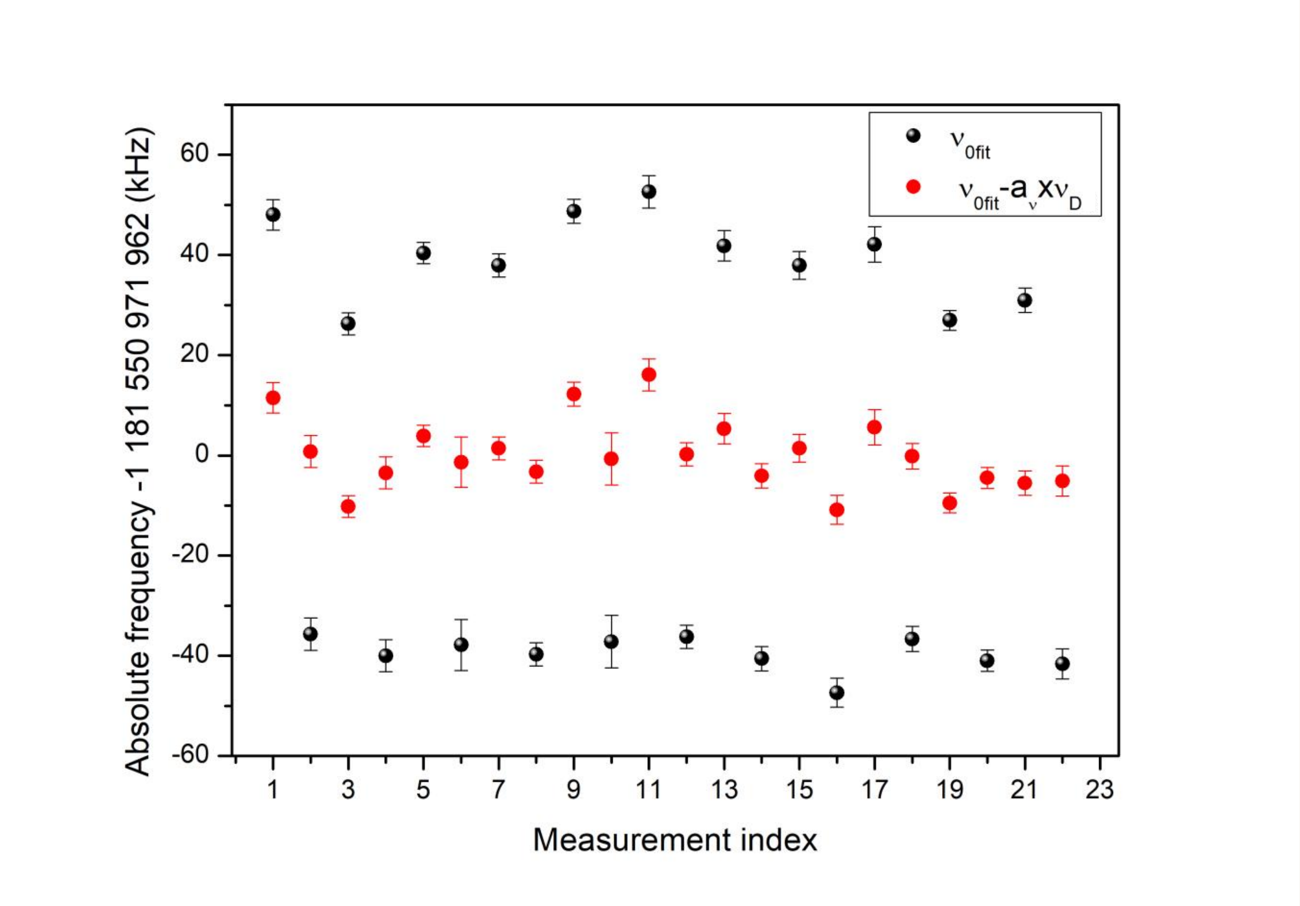

Frequency shift due to the finite detection bandwidth:

$$\nu_{0fit} = \nu_0 + a_\nu \times \nu_D,$$

$$\nu_D = \frac{\tau_D}{Q} \times \frac{\Delta\nu}{\Delta t}$$

a_ν filter parameter ~0.6;
τ_D filter time constant = 100 ms;
Q filter quality factor = ½;

$$\frac{\Delta\nu}{\Delta t} = \pm 0.31\ MHz/s.$$

The frequency systematic deviation is ±37 kHz, which is in good agreement with the observed deviations.

$$\boldsymbol{\nu_{200_{Hg}} = (1181\,550\,971\,962 \pm 2)\ \mathrm{kHz}}$$

F. Rohart, S. Mejri, P. L. T. Sow, S. K. Tokunaga, C. Chardonnet, B. Darquié, H. Dinesan, E. Fasci, A. Castrillo, L. Gianfrani, and C. Daussy, Physical Review A **90**, 042506 (2014).

Results

Uncertainty budget
(corresponding to one standard deviation)

Source	Type A (kHz)	Type B (kHz)
Statistical reproducibility	**2-5**	
Frequency calibration		**3**
AC-Stark shift		**110-24**
Pressure shift		**5**
Overall combined uncertainty **110-25**		

Hg-He collision-induced frequency shift +4.5 kHz;
Hg-Hg collision-induced frequency shift -5.3 kHz.

$$\nu_{200_{Hg}} = (1181\,550\,971\,962 \pm 110)\ \text{kHz}$$
$$\nu_{202_{Hg}} = (1181\,545\,676\,397 \pm 25)\ \text{kHz}$$

Relative accuracy 9-2×10^{-11}

Isotope shift (kHz)

This work	Witkowski et al.*
$5\,295\,565 \pm 5_{stat} \pm 120_{syst}$	$5\,295\,413 \pm 110_{stat} \pm 180_{syst}$

The two measurements are in good agreement, their difference being 152 kHz.

*M. Witkowski *et al*, Optics Express **27**, 11069 (2019).

Conclusions

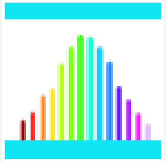

Using comb-calibrated wavelength-modulated saturated absorption spectroscopy, we have improved the current knowledge of the absolute frequency of the mercury intercombination line in the deep-UV, for the ^{200}Hg and ^{202}Hg isotopes.

We have reduced the statistical uncertainty by more than an order of magnitude, as compared to previous determinations.

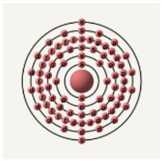

. As a result, the ^{200}Hg-^{202}Hg isotope shift could be measured more precisely and accurately, the statistical and systematic uncertainties being reduced by a factor of 22 and 1.5, respectively.

Outlooks

- Investigation of the AC-Stark frequency shift by repeating the measurements at different UV power levels.
- Doppler Broadening Thermometry measurements.